Experiments in Fluids (2019) 60:166
https://doi.org/10.1007/s00348-019-2815-1

RESEARCH ARTICLE

Generation of periodic gusts with a pitching and plunging airfoil

Nathaniel J. Wei[1,2] · **Johannes Kissing**[1] · **Cameron Tropea**[1]

Received: 18 May 2019 / Revised: 16 September 2019 / Accepted: 25 September 2019 / Published online: 22 October 2019

Abstract

The generation of smooth, symmetric, and periodic gust disturbances in an experimental context is demonstrated using a single oscillating airfoil. A pitching and plunging symmetric airfoil is suggested as a simpler alternative to existing gust-generation methods. The Theodorsen theory of unsteady aerodynamics is used as an analytical tool to dictate the kinematics necessary to produce periodic gusts with controlled waveform shape downstream of the airfoil. These analytic predictions improve the symmetry of fluctuations in the vertical velocity induced by the airfoil, as well as minimize the influence of vorticity shed by the oscillating airfoil. The apparatus is shown to produce smooth, symmetric gusts with high amplitudes and reduced frequencies compared to other gust-generation mechanisms in the literature. Furthermore, the control of downstream flow properties by airfoil motion kinematics has applications in experimental aerodynamics, the design of rotorcraft and light aerial vehicles, and biological propulsion.

Graphic abstract

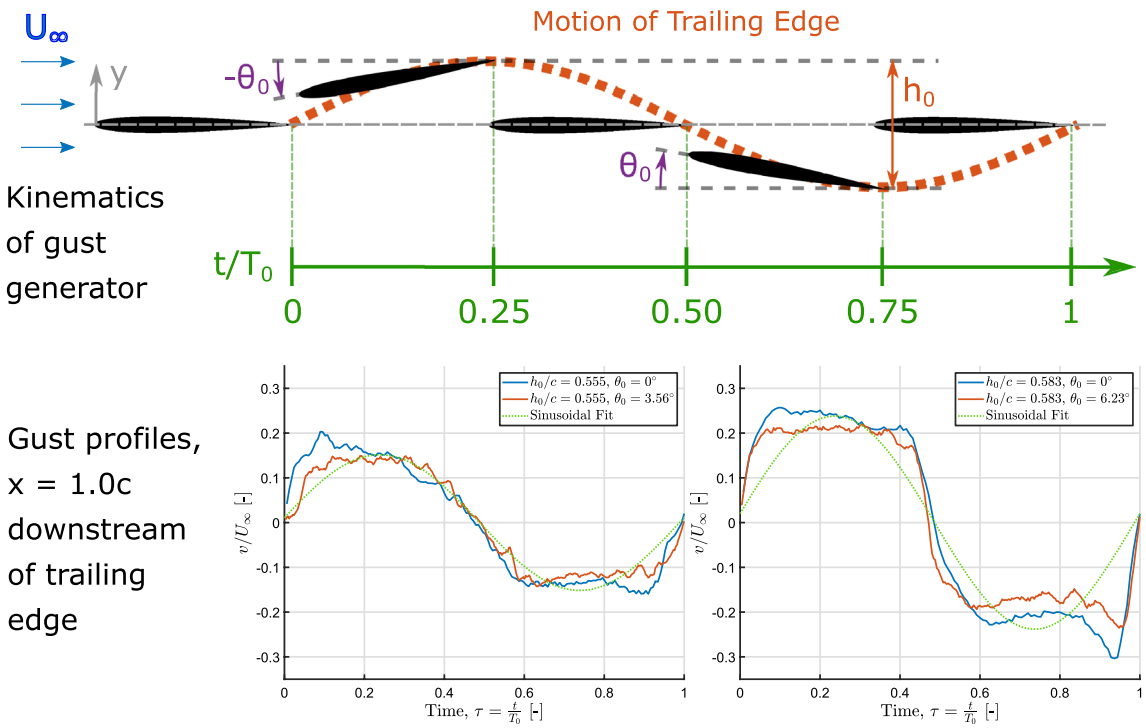

✉ Nathaniel J. Wei
njwei@stanford.edu

Extended author information available on the last page of the article

1 Introduction

The generation of well-defined periodic flow disturbances in a laboratory environment is a critical requirement for experiments involving unsteady aerodynamics, aircraft control, gust disturbances, unsteady sensor calibration, and many other applications. Modeling a periodic disturbance in simulations is comparatively easy: one must only specify a fluctuating velocity as an inflow condition, and the effects of the resulting flow can be studied directly, supposing that the correct boundary conditions for the outlet of the domain and for the surface of the test object are imposed. These can be treated in various ways depending on the type of solver employed and the nature of the problem being studied (e.g. Ekaterinaris and Platzer 1998; Visbal 2011). In experiments, however, generating the desired inflow conditions can be significantly more difficult. For example, gust disturbances of uniform character can be created from the turbulent fluctuations shed behind a passive grid (e.g. Lysak et al. 2016). In addition, active grids have demonstrated the ability to control the intensity and structure of turbulence in experimental settings (cf. Makita 1991; Cekli and van de Water 2010; Knebel et al. 2011; Griffin et al. 2019 etc.). These methods generate gust disturbances over a continuous spectrum. In many cases, however, it is desirable to produce disturbances at a single frequency. For example, a number of methods exist for generating vortical structures at a given frequency. Vortex shedding behind large cylinders or pylons yields periodic fluctuations in velocity that can be used in experiments (cf. Larose 1999), though a precise determination of the shedding frequency can be difficult. The vortices shed by an impulsively plunging plate can also be used to represent gust disturbances (Hufstedler and McKeon 2019).

Nevertheless, for numerous applications, a sinusoidal gust is required. The Sears function, for example, models unsteady loads on an airfoil for a sinusoidal gust disturbance in the normal velocity component (Sears 1941). This theory was extended by Goldstein and Atassi (1976) and Atassi (1984) to include sinusoidal velocity fluctuations in the streamwise as well as normal directions and has recently been re-examined by Wei et al. (2019). Sinusoidal gusts are also useful for tests of aircraft dynamics and controls, in which a series of well-defined, single-frequency disturbance inputs allows the frequency response of the system to be established (Bennett and Gilman 1966). The calibration of pressure transducers for unsteady conditions may also be achieved using a smooth, sinusoidal velocity signal.

The usefulness of sinusoidal gust disturbances in experimental investigations has led to the development of several methods for generating them. One of the earliest and simplest generators, constructed by Hakkinen and Richardson (1957), involved a plunging plate in a wind tunnel. The apparatus was used in an attempt to experimentally validate the Sears function, but proved unsatisfactory due to sensor noise. Subsequent gust-generation systems, possibly inferring that a single actuated plate was not sufficient for producing well-defined gusts, became more and more complex. Bennett and Gilman (1966) used four plates, mounted in pairs on the walls of a wind tunnel and actuated together by a series of linkages, to produce sinusoidal gusts for experiments with scale models of aircraft. Ham et al. (1974) and Jancauskas and Melbourne (1986) generated gusts using a pair of controlled-circulation airfoils. The concept was extended by Tang et al. (1996) in an array of four such airfoils. Approaches using arrays of six or more vanes (e.g. Saddington et al. 2015; Cordes et al. 2017; Wei et al. 2019) have been tested, though the wakes of the vanes tend to introduce turbulent fluctuations into the downstream flow conditions. Simpler generation mechanisms involving two pitching plates (e.g. Lancelot et al. 2015; Wood et al. 2017) avoid wake effects by construction, but tend to be limited in both the amplitude of the gusts produced and reduced frequency they can achieve. However, this design has been proven to be effective in transonic wind tunnels (Brion et al. 2015). Notably, in none of the aforementioned studies is the precise character of the gust disturbance analyzed or controlled; a periodically fluctuating velocity component with alternating peaks and troughs is typically deemed sufficiently sinusoidal. Alternatively, a single pitching airfoil has been demonstrated in many contexts to be sufficient for generating vortical gust disturbances, where smooth, sinusoidal disturbances are not required and wake effects do not need to be controlled (Klein et al. 2014, 2017).

The question of generating well-defined gusts using a single oscillating plate or foil should not be resolved by mere convention or consensus, especially since there are several advantages to such an apparatus for experiments. A single foil produces far less blockage in a wind tunnel than more complicated gust-generation devices. The actuation is also far simpler and less costly, and facilitates operation, maintenance, and removal. Finally, the simple actuation mechanism of the foil means that the parameter space that must be traversed to characterize the gust generator is significantly smaller than that of multi-vane devices or active grids, for example.

In the present study, a theory for the generation of smooth, symmetric, and periodic gusts with a single oscillating foil is proposed and validated with wind-tunnel experiments. The theory is developed from analytical, physical, and experimental arguments. Its effectiveness in producing tailored periodic profiles that exhibit minimal disturbance from the wake of the foil itself is then demonstrated. This

gust generator is able to produce gusts of controlled character over a range of frequencies and amplitudes and lends itself to experiments that require well-defined unsteady conditions.

2 Theoretical considerations

In this section, several considerations from the literature regarding the wakes of oscillating airfoils are discussed. These ideas undergird the hypothesis that the generation and control of well-defined periodic gusts is possible with a single airfoil as a gust generator. A theory for the generation of these gusts is then developed from the Theodorsen model for unsteady aerodynamics. These theoretical considerations provide guidance for the experiments that follow.

2.1 Considerations from the literature

To generate smooth, symmetric, and periodic gusts with a single airfoil, inspiration is derived from studies regarding the aerodynamics of oscillating airfoils. Anderson et al. (1998) characterized the wake patterns behind a NACA-0012 airfoil actuated in pitch and plunge over a range of reduced frequencies, $k = \frac{\omega c}{2U_\infty}$, and Strouhal numbers, $St = \frac{fA}{U_\infty}$. Here, $\omega = 2\pi f$ is the frequency of oscillation in radians per second, and A represents the characteristic width of the wake, estimated by the plunge amplitude or the trailing-edge amplitude of the airfoil. For a range of combinations of pitch and plunge amplitudes, several distinct wake regimes were identified. Of particular interest to this study is the region defined by Strouhal numbers less than 0.2 and pitch amplitudes less than 50°, in which a "wavy wake" without significant vortex shedding was observed. The implied periodicity of the wake fluctuations and the lack of strong unsteady flow phenomena highlight this regime as one that would be particularly well-suited for the purpose of generating and controlling smooth, periodic gust waveforms with a single airfoil. This result suggests that the formation of well-defined quasi-sinusoidal oscillations in the wake of an airfoil can be achieved systematically as a function of pitch and plunge kinematics.

Two subsequent studies analyzed the effects of airfoil kinematics on wake structures generated by a pitching and plunging airfoil. For pitching and plunging airfoils, these wake structures are predominantly formed in dynamic stall, where strong leading-edge vortices (LEVs) and trailing-edge vortices (TEVs) roll up on and behind the airfoil, and convect downstream into the wake (Carr 1988). Rival et al. (2009) studied the effects of non-sinusoidal actuation profiles on the propagation of these structures into the wake, demonstrating that the strength of the LEV on the airfoil and its persistence into the wake were affected by the shape of the motion waveforms followed by the airfoil. Extending this result, Prangemeier et al. (2010) demonstrated that the addition of a quick pitch-down motion in the downstroke of an oscillating airfoil served to decrease the circulation of the TEV by as much as 60%. The additional pitch motion of the airfoil interfered with the formation of the TEV, so that the strength of the TEV was not significantly dependent on the characteristics of the LEV. Similar reductions in wake vorticity were demonstrated in numerical simulations by Gharali and Johnson (2013). Therefore, though the strengths of LEVs and TEVs are inherently connected, the addition of pitching motions for a plunging airfoil can inhibit the generation of large trailing-edge vorticity in spite of large accumulations of vorticity at the leading edge. This is instructive to the current study, because the shedding of large, intermittent velocity fluctuations is antithetical to the generation of smooth, periodic velocity signals downstream.

To minimize vorticity effects in the flow downstream of the gust generator, the wake of the generator itself should be minimized along with the persistence of dynamic effects. To this end, Hufstedler and McKeon (2019) developed a vortical gust generator using an impulsively plunging plate. The plunging motions of the plate meant that the wake vorticity from the plate had a limited effect on the gust region, since the wake vorticity would only cross through the measurement domain twice per cycle. This is in contrast to gust generators that employ purely pitching vanes, which are fixed in place, and thus continually disturb the downstream flow conditions.

These considerations, taken together, imply that the generation of gusts with smooth, symmetric waveforms is possible with a single airfoil, provided the kinematics of that airfoil are carefully controlled. Relatively low Strouhal numbers and reduced frequencies are required to mitigate vortex shedding due to dynamic-stall flow phenomena. Plunge oscillations can help reduce the effects of the airfoil's wake on the downstream flow properties. Adding pitch motions can further attenuate trailing-edge vorticity, thereby reducing intermittency in the downstream velocity signals.

The remainder of this work is therefore concerned with the combination of these observations: specifically, which combinations of pitch and plunge produce satisfactorily smooth, approximately sinusoidal velocity fluctuations for a range of Strouhal numbers and reduced frequencies. To achieve these gust conditions, intermittent effects from vortices shed by the gust generator should be avoided, and the resulting velocity profiles should be as symmetric and regular as possible. These criteria will drive the development and characterization of a robust theory for gust generation with a single airfoil.

In this study, gust fluctuations in the flow-normal direction are specifically investigated. Fluctuations in the

streamwise velocity and in the flow vorticity were not central to the applications of this work, and measurements of these quantities demonstrated that they were insensitive across the range of parameters tested in these experiments. Additionally, Wei et al. (2019) have shown that, in the case of the Sears function, streamwise velocity fluctuations are not critical to obtaining experimental convergence with analytical predictions. Thus, gust fluctuations in the flow-normal direction are the main quantity of interest in this work.

2.2 Adaptation of the Theodorsen theory for the generation of periodic gusts

Theodorsen (1934) developed a first-order theory for the forces and moments experienced by a pitching and plunging flat-plate airfoil. The theory combines added-mass forces from the pitch (θ) and plunge (h) motions of the airfoil with the influence of the circulation in the wake to predict the unsteady aerodynamic loads on the airfoil. Since the theory accounts for the effects of both kinematics and wake circulation, it can be used to build a relation for the kinematic parameters needed to generate smooth, periodic gusts. It has also been validated in the same experimental apparatus used in the present study (Cordes et al. 2017). The theory was used by Brion et al. (2015) to estimate the amplitude of gusts produced by a purely pitching airfoil in transonic flow. Apart from this, it has been absent from the gust-generation literature.

The pitching moment on the airfoil is of particular interest because it provides a connection between airfoil dynamics and downstream flow characteristics. While the Theodorsen theory does not model dynamic effects, the vortices associated with dynamic stall should not be present in the ideal gust-generation case, and thus the forces and moments on the airfoil should be captured well by the Theodorsen function. In this ideal case, the airfoil would simply redirect flow up and down, creating vertical fluctuations in velocity without introducing significant circulation into the downstream region. The leading edge of the airfoil would minimally disturb the incoming flow, so that the flow on the upper and lower surfaces of the airfoil follow the airfoil's surface without significant differences between the upper and lower surface. The resulting lack of velocity gradients at the trailing edge of the airfoil would then minimize the circulation injected into the wake. In this sense, both the added-mass moments and moments due to wake circulation would be optimally small, and the total pitching moment on the airfoil would be minimized.

The kinematics required to achieve this ideal gust-generation case can be calculated using Theodorsen's theory. For a given plunge amplitude h_0, inflow velocity U_∞, and gust frequency f, it is possible to find the pitch amplitude θ^* that will minimize the amplitude of the pitching moment on the airfoil. The plunge amplitude is defined in this case by the peak-to-peak excursion distance of the trailing edge of the airfoil, as in Anderson et al. (1998), so that the length scale within the Strouhal number approximately represents the width of the airfoil's wake. The equation for the pitching moment is given in terms of these parameters as

$$\begin{aligned} M_\theta = &-\rho b^2\left[\pi\left(\frac{1}{2}-a\right)Ub\dot{\theta}+\pi b^2\left(\frac{1}{8}+a^2\right)\ddot{\theta}-a\pi b\ddot{h}\right] \\ &+2\rho Ub^2\pi\left(a+\frac{1}{2}\right)C(k)\left[U\theta+\dot{h}+b\left(\frac{1}{2}-a\right)\dot{\theta}\right], \end{aligned} \tag{1}$$

where b is the half-chord of the airfoil, $a \in [-1, 1]$ is the center of rotation of the airfoil (nondimensionalized by b), θ is the pitch angle of the airfoil, h is the plunge location of the airfoil (positive downward), U is the free-stream velocity, and ρ is the density of the working fluid. In this case, we define the pitching moment about the trailing edge, corresponding to $a = 1$, to quantify the cumulative influence of the airfoil on the flow from the leading edge up to the trailing edge. The Theodorsen function $C(k)$ is a function only of the reduced frequency $k = \frac{\omega b}{U}$, and has both real and imaginary components, i.e. $C(k) = F(k) + iG(k)$. These functions are defined in the original work by Theodorsen (1934). Since $C(k)$, and thereby $F(k)$ and $G(k)$, does not depend on θ, these functions do not factor into the optimization of the pitch amplitude, θ_0, undertaken here.

To calculate the optimal pitch amplitude for gust generation, θ^*, we define the kinematics of the airfoil and their time derivatives as sinusoidal waveforms in the complex plane (following McGowan et al. 2011):

$$\begin{aligned} h = -\frac{h_0}{2}e^{i\omega t}, \quad \dot{h} = -i\omega\frac{h_0}{2}e^{i\omega t}, \quad \ddot{h} = \omega^2\frac{h_0}{2}e^{i\omega t}; \\ \theta = \theta_0 e^{i\omega t}e^{i\phi}, \quad \dot{\theta} = i\omega\theta_0 e^{i\omega t}e^{i\phi}, \quad \ddot{\theta} = -\omega^2\theta_0 e^{i\omega t}e^{i\phi}. \end{aligned} \tag{2}$$

Here, ϕ is the phase offset of θ with respect to h. The time-dependent pitching moment can be written as $M_\theta = \hat{M}_\theta e^{i\omega t}e^{i\psi}$, so that the time-dependent portion of the waveforms can be removed. Additionally noting that $\omega = \frac{kU}{b}$, Eq. 1 can be written as

$$\begin{aligned} \frac{\hat{M}_\theta e^{i\psi}}{\pi\rho b^2U^2} = &\left(a-\frac{1}{2}\right)k\theta_0 e^{i\phi}i+\left(\frac{1}{8}+a^2\right)\theta_0 k^2 e^{i\phi} \\ &+\frac{a}{2b}k^2h_0+2\left(a+\frac{1}{2}\right)(F(k)+iG(k)) \\ &\left[\theta_0 e^{i\phi}-i\frac{kh_0}{2b}-\left(\frac{1}{2}-a\right)k\theta_0 e^{i\phi}\right]. \end{aligned} \tag{3}$$

The square of the magnitude of this complex expression reduces to a quadratic function in θ_0, after a rather unpleasant amount of algebra:

$$\left(\frac{\hat{M}_\theta}{\pi\rho b^2 U^2}\right)^2 = \left(C_R^2 + C_I^2\right)\theta_0^2 + 2\left(C_R D_R + C_I D_I\right)\theta_0 + D_I^2, \tag{4}$$

where

$$\begin{aligned} C_R =& k\left[\left(a-\frac{1}{2}\right)\sin(\phi) + \left(\frac{1}{8}+a^2\right)k\cos(\phi)\right] \\ &+ F(k)\left[3\cos(\phi) - 2\left(\frac{1}{4}-a^2\right)k\sin(\phi)\right] \\ &- G(k)\left[3\sin(\phi) + 2\left(\frac{1}{4}-a^2\right)k\cos(\phi)\right], \\ C_I =& k\left[\left(\frac{1}{2}-a\right)\cos(\phi) + \left(\frac{1}{8}+a^2\right)k\sin(\phi)\right] \\ &+ F(k)\left[3\sin(\phi) + 2\left(\frac{1}{4}-a^2\right)k\cos(\phi)\right] \\ &+ G(k)\left[3\cos(\phi) - 2\left(\frac{1}{4}-a^2\right)k\sin(\phi)\right], \\ D_R =& \frac{a}{2b}k^2 h_0 + \left(a+\frac{1}{2}\right)\frac{kh_0}{b}G(k), \text{ and} \\ D_I =& -\left(a+\frac{1}{2}\right)\frac{kh_0}{b}F(k). \end{aligned} \tag{5}$$

D_R and D_I can be written in terms of k and St, so that the four coefficients given in Eq. 5 are only functions of k, St, ϕ, and a:

$$\begin{aligned} D_R =& \pi a k St + 2\pi St\left(a+\frac{1}{2}\right)G(k), \\ D_I =& -2\pi St\left(a+\frac{1}{2}\right)F(k). \end{aligned} \tag{6}$$

To minimize the pitching moment, we take the derivative of its magnitude with respect to the pitch amplitude and set this derivative equal to zero:

$$\frac{\partial \hat{M}_\theta}{\partial \theta_0} = 0. \tag{7}$$

The solution is easily found as

$$(\theta_0)_{min} = \theta^* = -\left[\frac{C_R D_R + C_I D_I}{C_R^2 + C_I^2}\right]. \tag{8}$$

θ^* is thus the pitch amplitude that produces the minimum pitching moment $\hat{M}_\theta^*$ for a given combination of k, St, a, and ϕ. For the reasons outlined previously, we have chosen $a = 1$ in this study, which means θ^* and the corresponding $\hat{M}_\theta^*$ are functions of k, St, and ϕ only. Selecting a set of plunge kinematics determines k and St, leaving ϕ as the remaining free parameter. Thus, for any given phase offset ϕ, the pitch amplitude θ^* that produces the minimum pitching moment $\hat{M}_\theta^*$ can be calculated using Eq. 8. The variations of θ^* and $\hat{M}_\theta^*$ with ϕ are shown in Fig. 1 for a given set of dynamic parameters ($k = 0.603$, $St = 0.096$). From this figure, it is clear that while each selection of ϕ has a corresponding minimized pitching moment $\hat{M}_\theta^*$, there exists a value of ϕ that has a lower associated optimal pitching moment than all others. In the case shown in Fig. 1, this phase offset is $\phi^\dagger = 113.7°$, with a corresponding pitch amplitude of $\theta^* = 14.25°$ and precisely zero pitching moment about its trailing edge. This condition of zero pitching moment for a particular $\phi^\dagger$ exists for every combination of k and St, and according to the arguments put forth previously in this section, would be optimally conditioned to produce smooth, periodic gusts with minimal interference from the airfoil itself.

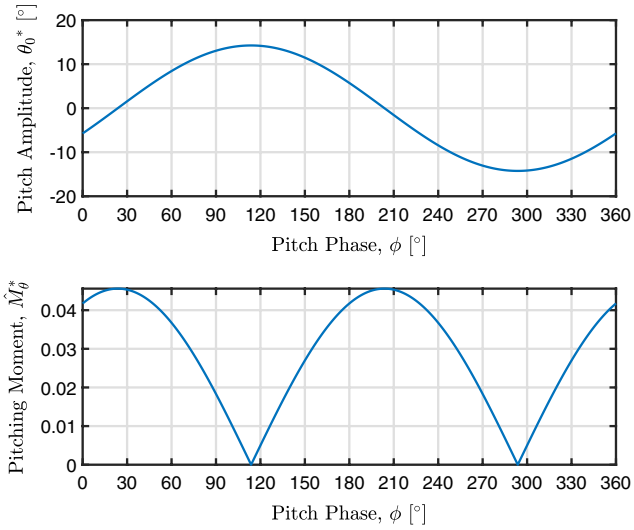

Fig. 1 Variations of the optimal pitch amplitude θ^* and resulting minimized pitching moment $\hat{M}_\theta^*$ with pitch phase ϕ, for $St = 0.096$ and $k = 0.603$. The global minimum pitching moment for this case occurs at $\phi^\dagger = 113.7°$. A phase ϕ_i with $\theta^*(\phi_i) < 0$ is equivalent to a phase of $\phi_i \pm 180°$ and amplitude of $|\theta^*|$

In practice, however, one may not be able to select any desired phase offset due to actuation constraints. In the experiments presented in this study, the airfoil was actuated with two separate linear actuators that were each controlled with sinusoidal waveforms. This setup restricted the accessible phase offsets to 0° and 180°. Though these values of ϕ do not result in zero pitching moment, the θ^* values from the theory still produce the lowest possible pitching moment given the constraints on ϕ; the experiments presented in this work aim to show that this moment-minimization scheme produces the most optimal gusts for any desired combination of k, St, and ϕ. Figure 1 shows that at $\phi = 0°$ and $\phi = 180°$, the minimized pitching moment has the same value, but the sign of θ^* at $\phi = 0°$ is negative. Since the pitch waveform

is sinusoidal, a negative amplitude is equivalent to a positive amplitude with a 180° phase shift. The $\phi = 0°$ case with $\theta^* < 0$ is thus equivalent to the $\phi = 180°$ case with $\theta^* > 0$: both describe a scenario in which the pitch waveform is out of phase with the plunge waveform. Therefore, there exists no positive pitch amplitude that will minimize the pitching moment for $\phi = 0°$, and moreover, employing pitch in phase with plunge should not be conducive to the production of smooth, controlled gusts. Given these constraints on the pitch phase, optimal pitch amplitudes for several sets of airfoil kinematics are given in Tables 2 and 3 in Sect. 4.2.

In this section, we have outlined an analytical method for establishing pitch kinematics for a given reduced frequency and Strouhal number that will produce regular, well-defined periodic gusts. These results are notably only indirectly dependent on the Reynolds number, through the dependence of k and St on U_∞ and c. This series of assumptions and arguments for gust generation are theoretical in nature and require experimental investigation to verify whether they apply in practice. The character of the gusts produced by such a gust generator provides the validation criteria for the theory. In particular, the sinusoidal character of the velocity profiles and the extent of the wake of the airfoil downstream of the gust generator will serve as indicators for the quality of the gusts generated according to these principles.

3 Experimental setup

In this section, the experimental apparatus used in this study is described in detail. The processing of raw data from the experiment is outlined, and two metrics for quantifying the character of gusts are explained.

3.1 Experimental apparatus

The experiments described in this work were carried out in an open-return wind tunnel at the Technische Universität Darmstadt. This tunnel had a square test section with a side length of 0.45 m. Optical access was provided by a removable glass plate that spanned the length of the test section, as well as a window on the top of the test section through which the laser sheet for the PIV system was passed. The flow velocity in the tunnel was held at $U_\infty = 2.5 \pm 0.1$ m/s using a closed-loop controller and an impeller anemometer (type TS16/15GE- mc40A/125/p0/ZG1) from Höntzsch GmbH installed near the inlet of the test section. This corresponded to a chord-based Reynolds number of about 20,000. Turbulence intensities in the test section were measured to be less than 2%. More details on the wind tunnel can be found in Rival et al. (2009).

The test airfoil used in this study was a symmetric NACA-0008 profile with a chord of $c = 120$ mm and thickness of $\delta_{foil} = 9.6$ mm. The airfoil was 3D-printed and reinforced in the spanwise direction with two carbon-fiber struts to inhibit elastic deformations. Two halves were printed, laminated in black foil to reduce reflections from the PIV laser light sheet, and attached to an aluminum mount, which was also laminated in black foil. The mount was supported by two LinMot PS01-48x240F-C linear actuators, having a dynamic position accuracy of ±0.1 mm. These were controlled from a computer using the LinMot-Talk program, and were preloaded with sinusoidal motion profiles for each experiment according to the required pitch and plunge kinematics. They could be used to actuate the airfoil in pitch and plunge at frequencies of up to 10 Hz. The downstream actuator was centered on the airfoil's trailing edge. A schematic of the actuators and test airfoil is given as Fig. 2.

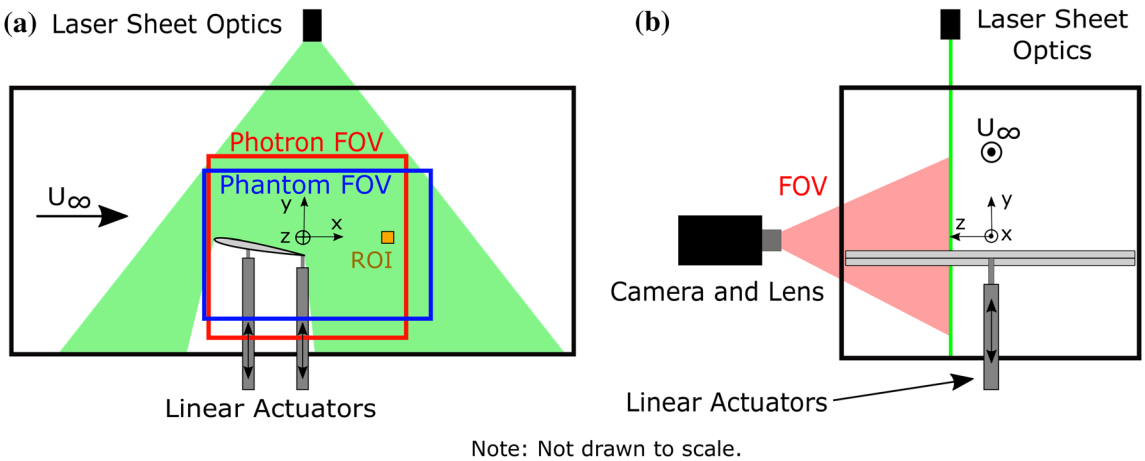

Fig. 2 Schematic of the experimental setup: **a** side view, and **b** rear view. Fields of view of the two cameras are shown in (**a**). The region of interest (ROI) used to measure velocity and vorticity profiles is shown as an orange square in (**a**)

Flow-field measurements in this study were acquired using particle-image velocimetry (PIV). Seeding particles were generated from Di-Ethyl-Hexyl-Sebacat (DEHS), which had a mean diameter of $0.5 - 1.5\ \mu$m and a response time of $\tau_s = 2.7\ \mu$s (Raffel et al. 2007). The laser sheet was produced by a Litron LDY-303 high-speed dual-cavity Nd:YLF laser with a wavelength of 527 nm and frequency of 1 kHz. The sheet was generated by cylindrical lenses mounted high above the test section, to provide as large a field of view as possible. It was positioned at the edge of the optical-access window at the top of the test section, corresponding to a location of 20% of the airfoil's span from the midpoint. Due to the high power of the laser, an additional strip of fluorescent foil was wrapped around the airfoil at the location of the laser sheet, to further reduce reflections in the images and to prevent the laser sheet from burning into the airfoil itself. The location of the laser sheet is shown in Fig. 2. A larger field of view was not possible, as the laser had to be operated at full power in the given configuration to sufficiently illuminate seeding particles in the flow.

Images were captured at a double-exposure repetition rate of 1 kHz using a high-speed camera. In the first round of experiments, a Phantom v 12.1 camera was used. Repairs on the lab's Photron SA 1.1 camera were complete for the second round of experiments. A band-pass filter was applied with the Photron camera to further protect the camera sensor from reflections, as well as to mitigate glare from reflections on the airfoil's surface. For both cameras, a Zeiss 50-mm lens was used. The approximate fields of view for both cameras are shown in Fig. 2b. The cameras were mounted on a traverse, and the scale was computed using a target placed in the laser sheet. The camera, laser cavities, and actuators were all controlled with a LabVIEW script using a National Instruments PCI-6220 data-acquisition card. This allowed the measurements and data collection to be centrally synchronized using digital pulses. Additional details regarding differences in the setup between the two rounds of experiments are given in Table 1.

3.2 Data processing and analysis

Two-component velocity fields were obtained from the raw images using the PIVview2C software package from PIVTEC GmbH. In both cases, a multigrid approach with three iterations was applied, with 50% overlap between correlation windows. Window sizes were selected so that, on average, about 10 particles could be found in each interrogation area (Tropea et al. 2007). Outlier detection and median filtering with 3×3 px windows were executed on the resulting vector fields. Specific details regarding processing parameters for the two rounds of experiments are given in Table 1.

The location of interest within the flow field for these experiments was a point one full chord length downstream of the trailing edge of the airfoil. This was selected with an eye towards future experiments: the experimental setup had been originally designed to study two oscillating airfoils in a tandem configuration (Rival et al. 2011), and the location of the leading edge of the downstream airfoil was 120 mm downstream of the trailing edge of the forward airfoil. Additionally, one chord length into the wake represented an intermediate distance at which the influences of neither transient effects nor viscous dissipation were significant. In future studies, it may be useful to investigate whether the results presented here hold also in the far-wake region. For

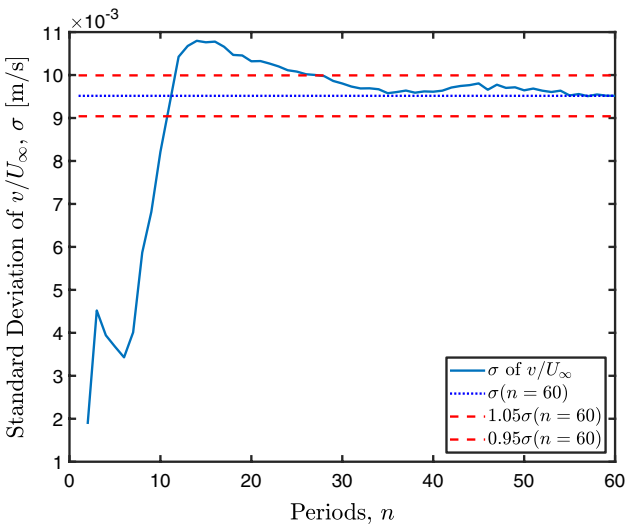

Fig. 3 Standard deviation of the vertical velocity at $\frac{t}{T_0} = 0.8$ for $St = 0.096$ and $k = 0.603$, as a function of the number of test periods. Acceptable convergence is achieved by 30 periods

Table 1 Camera and PIV processing parameters for the two rounds of experiments presented in this work

Property	Round 1	Round 2
Camera	Phantom v12.1	Photron SA1.1
Resolution (px)	1280×800	1024×1024
Scale (px/mm)	3.630	2.833
Frame-straddling interval (μs)	400	450
Cross-correlation window size (px)	32×32	16×16
Peak-finding algorithm	3×3 Gaussian fit	Whittaker reconstruction

most of the results in this work, a square box of length 15 mm within the measurement plane was isolated at $x = 1.0c$ behind the test airfoil for the purpose of characterization of the gust signal, through averaging all velocity vectors within the region. This region of interest (ROI) was located at the same height as the midpoint of the plunge amplitude of the airfoil, defined as $y = 0$, and is represented schematically as an orange box in Fig. 2a. In Sect. 4.3, an ROI located at $x = 1.5c$ behind the test airfoil was used to evaluate the evolution of the gusts as they were convected downstream.

To determine the number of test periods required to achieve statistical significance, the vertical velocity v at one instance of time within a test period was averaged over 60 periods at the point described above. A protocol with a large plunge amplitude ($h_0/c = 0.5$) and zero pitch was used to ensure that dynamic effects would be present and would be incorporated into the analysis. The averaged values for each period were randomly sampled to determine the convergence of the standard deviation $\sigma(n)$ with the number of periods n included in the phase-average. One thousand bootstrap samples were taken for each value of n, and an estimate for the population standard deviation was computed from these samples (cf. Efron 1979). The results from this analysis, shown in Fig. 3, revealed that $n = 30$ test periods yielded reasonable convergence in the standard deviation (within $\pm 5\%$ of the final value, $\sigma(n = 60)$). Thus, all data presented in this work are phase-averaged over at least 30 test periods. Furthermore, at the start of every experiment, the airfoil was oscillated through a few unrecorded motion periods to ensure that startup effects did not influence the phase-averaged data.

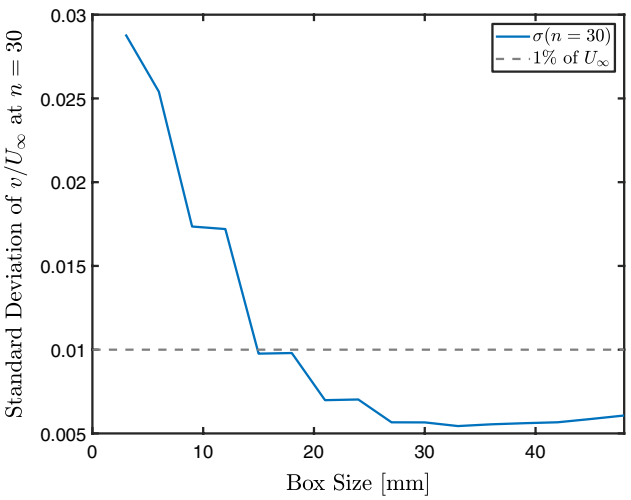

Fig. 4 Standard deviation of 30 phase-averaged vertical-velocity measurements within the region of interest (ROI) at $\frac{t}{T_0} = 0.8$ for $St = 0.096$ and $k = 0.603$, as a function of the side length of the ROI. Statistical convergence is maintained if an ROI dimension of 15 mm is selected

Using this number of phase-averaged test periods, the choice of the dimension of the ROI was then validated. Again using the bootstrap method with one thousand random samples, the standard deviation of the velocity vectors located within the ROI was computed for several ROI box sizes. The results of this analysis, shown in Fig. 4, confirmed that a dimension of 15 mm produced a standard deviation in v below 1% of the free-stream velocity. Thus, this dimension was selected to maintain a high degree of statistical convergence while keeping the ROI small enough to represent a point measurement.

Finally, to quantify the two main parameters of interest for the gust-generation problem, two methods for analysis were developed. To quantify the character of the waveforms of the velocity fluctuations, the average acceleration at the theoretical peaks of the signal was measured using linear fits about $\frac{t}{T_0} \approx 0.25$ and $\frac{t}{T_0} \approx 0.75$. The dimensionless time $\frac{t}{T_0}$ was given by the total period T_0 and was phase-referenced to the sine function. The fits encompassed 10% of T_0 on either side of the instant of interest. After correcting for sign, the slopes of these two linear fits were averaged. For an ideal profile, this metric would yield a mean acceleration of $\frac{dv}{dt} = 0$ m/s^2, indicating symmetry in the velocity profiles. The idea is illustrated in Fig. 9 in the following section.

To quantify the influence of shed vortices in the wake of the airfoil on the region downstream of the gust generator, the vertical extent of the wake vorticity was measured at the location of interest, $x = 1.0c$. For every time instant in the phase-averaged period, vectors of vorticity at $x = 1.0c$ and y spanning the height of the domain were taken. These vectors were compiled into a 2D field in y and t to show the evolution of the thickness of the wake region over one period. The vorticity fields were smoothed using a 3×3 filter, to compensate for the effects of numerical differentiation. An automatically adaptive threshold based on the standard deviation across the entire y-t field to binarize the field, followed by a 2D 7×7 median filter and hole-filling method, was employed to identify and isolate areas of relatively high vorticity. The result of this procedure was an automatically generated mask that isolated the wake of the airfoil from the rest of the measurement domain. The width of the wake vorticity profile that was left after the mask had been applied was measured at every time instant across the phase-averaged cycle, and these values were then averaged to represent the mean width of the wake. Examples of vorticity profiles after application of the mask will be shown later in Fig. 11. In the ideal case, this metric would be minimized, indicating minimally low interference of the gust generator itself on the flow downstream of the wake.

4 Experimental results

In this section, the arguments put forward in Sect. 2.2 are examined experimentally. First, various experiments are performed to establish a baseline for effects of airfoil kinematics on the character of the gusts produced. Based on these baseline cases, a template for the kinematics of the gust generator is proposed, which arises from the conclusions of the theoretical analysis. The predictions of the Theodorsen theory as applied to gust generation are tested using the metrics outlined in Sect. 3.2 to demonstrate that gusts with a satisfactorily smooth and symmetric character can be produced using a single pitching and plunging airfoil. Finally, the effects of the gust generator on fluctuations of the streamwise velocity and spanwise vorticity are analyzed, and the effectiveness and limitations of the gust-generation scheme with regard to other measurement locations and conditions are evaluated.

4.1 Baseline cases

To understand the effects of the various free parameters in the kinematics of a pitching and plunging airfoil on the vertical velocity signal in the wake, a series of concise parametric studies was conducted. First, the two dimensionless parameters governing the dynamics of the oscillating airfoil, St and k, were varied independently for an airfoil moving in pure plunge. For $k = 0.603$, the plunge amplitude of the airfoil was varied to produce Strouhal numbers between 0.032 and 0.112. The resulting velocity profiles, taken at the region of interest specified in Sect. 3.2, are shown in Fig. 5a. Conversely, for $St = 0.080$, the reduced frequency was varied between 0.302 and 0.905. These baseline conditions ($St = 0.080$, $k = 0.603$) represent moderate values of k and St for the range of parameters tested in this study, which allowed the effects of each of these parameters to be observed independently. The velocity profiles for these experiments are shown in Fig. 5b. These experiments showed that the amplitude of the fluctuations in the vertical velocity ($\hat{v}$) was a strong linear function of Strouhal number and a weaker function of reduced frequency. These trends are shown explicitly in Fig. 17 for cases utilizing both pitch and plunge, and will be discussed in more detail in Sect. 4.3. In addition, most of the curves shown were asymmetric, with peaks occurring relatively early within each half-cycle, or more geometrically conceived, leftward-leaning maxima. This "leaning" behavior should be avoided if symmetric signals are desired. Finally, in many cases, the waveform was interrupted by a deviation around $\frac{t}{T_0} = 0.95$ that was not present in the corresponding positive half of the signal. This was likely an artifact of flow around the actuator mounts interfering with the wake, an unavoidable asymmetry in the present experiment. Thus, though the negative portions of the waveforms show similar trends to the positive portions, the positive halves of the velocity profiles should be viewed as more reliable indicators of trends than the negative halves.

Next, the effect of pure pitch on wake character was studied. The airfoil was pitched through $5° \leq \theta_0 \leq 15°$, first about its leading edge and then about its trailing edge. The reduced frequency was again $k = 0.603$. The resulting

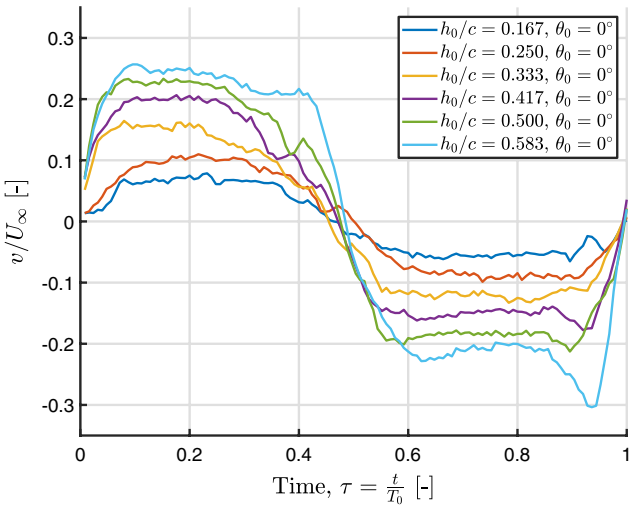

(a) $0.032 \leq St \leq 0.112$ and $k = 0.603$

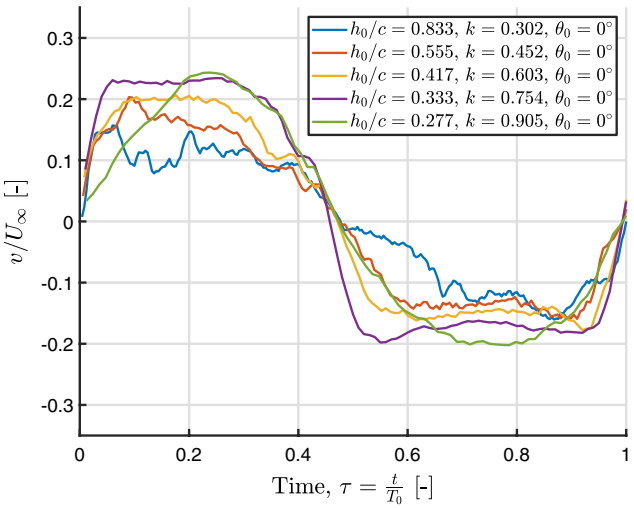

(b) $0.302 \leq k \leq 0.905$ and $St = 0.080$

Fig. 5 Baseline profiles of vertical velocity v for a purely plunging airfoil for a range of **a** Strouhal numbers and **b** reduced frequencies. Measurements were taken one chord behind the airfoil's trailing edge, and were phase-averaged over 30 cycles. The peaks of the profiles tend to be biased toward earlier dimensionless times

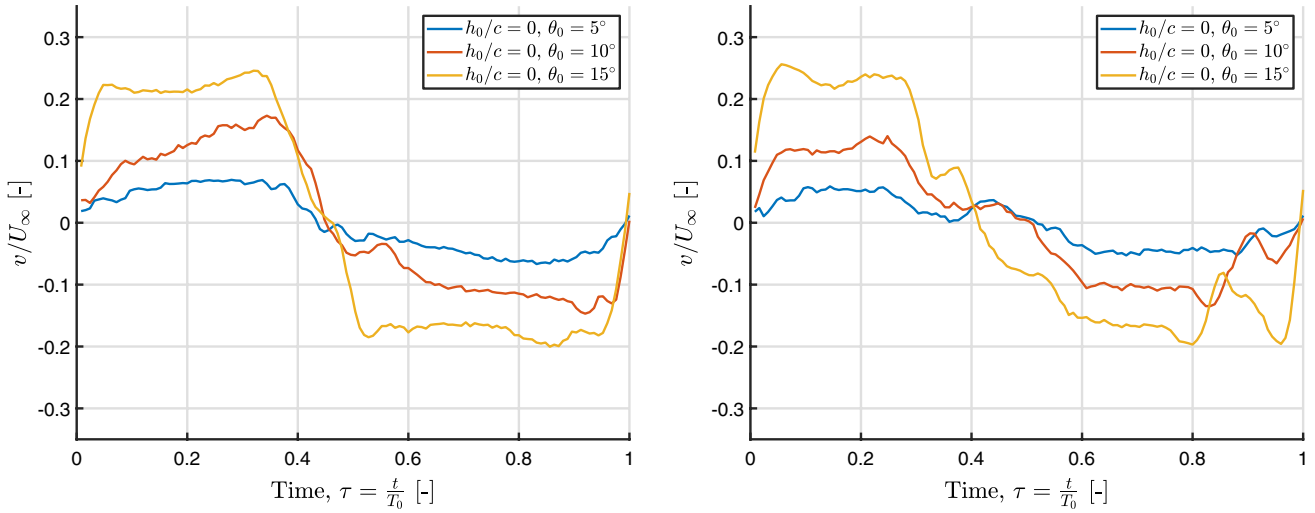

(a) Pure pitch about the leading edge **(b)** Pure pitch about the trailing edge

Fig. 6 Baseline profiles of v for a purely pitching airfoil ($k = 0.603$), rotating about its **a** leading edge and **b** trailing edge. The profiles appear to be more regular when leading-edge motion is minimized—achieved by the kinematics of (a) in this case

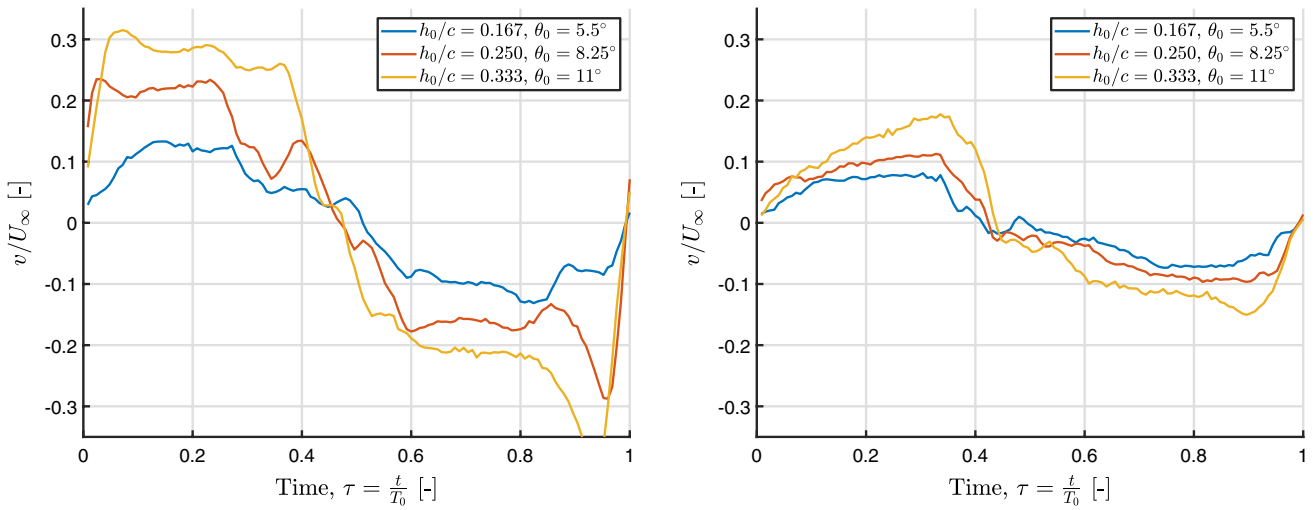

(a) $\phi = 0°$ (b) $\phi = 180°$

Fig. 7 Baseline profiles of v for a pitching and plunging airfoil ($k = 0.603$, range of St), with pitch phase **a** $\phi = 0°$ and **b** $\phi = 180°$. A phase of 180° results in more regular profiles (due to the reduction in leading-edge motion) and biases the waveform peaks toward later dimensionless times

profiles are shown in Fig. 6a and b. Upon inspection, pitching about the leading edge appeared to result in smoother, more regular profiles than pitching about the trailing edge. This was due to significant dynamic effects and resultant shedding of vortices instigated by large excursions of the leading edge of the airfoil that were observed in the velocity and vorticity fields when the airfoil was pitched about its trailing edge (cf. Widmann and Tropea 2015). Thus, it was concluded that excessive motions of the leading edge were counterproductive to the generation of smooth, well-defined velocity signals. Additionally, the velocity profiles in the case of pitch about the leading edge peaked later in each half-cycle. This suggested that the addition of pitch to plunge could potentially offset the leftward lean observed in Fig. 5.

A similar conclusion was drawn by combining pitch and plunge kinematics, and changing the phase offset between the two. At $k = 0.603$, a set of three increasing pitch amplitudes was combined with a proportionally increasing set of plunge amplitudes. This series was carried out with phases

of $\phi = 0°$ and 180°. Since the trailing-edge amplitude defined the plunge waveform, a phase of 0° produced larger excursions of the leading edge, and correspondingly less regular velocity profiles, as seen in Fig. 7a. Conversely, a phase of 180° resulted in smaller motions of the leading edge; the velocity profiles (shown in Fig. 7b) exhibited the same rightward-shifted maxima as in Fig. 6a.

The results observed in these small parametric studies suggested an ideal set of kinematics for the generation of smooth, symmetric gusts. Plunge motions allowed for higher gust amplitudes to be created, but introduced asymmetry

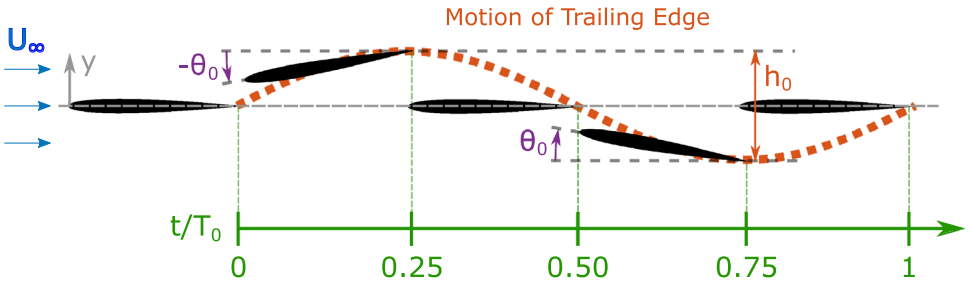

Fig. 8 Schematic of the kinematics employed for gust generation, as determined by the Theodorsen theory outlined in Sect. 2.2 and the set of test cases given in Tables 2 and 3. The sinusoidal waveform shown as a dashed orange line represents the motion of the trailing edge of the airfoil

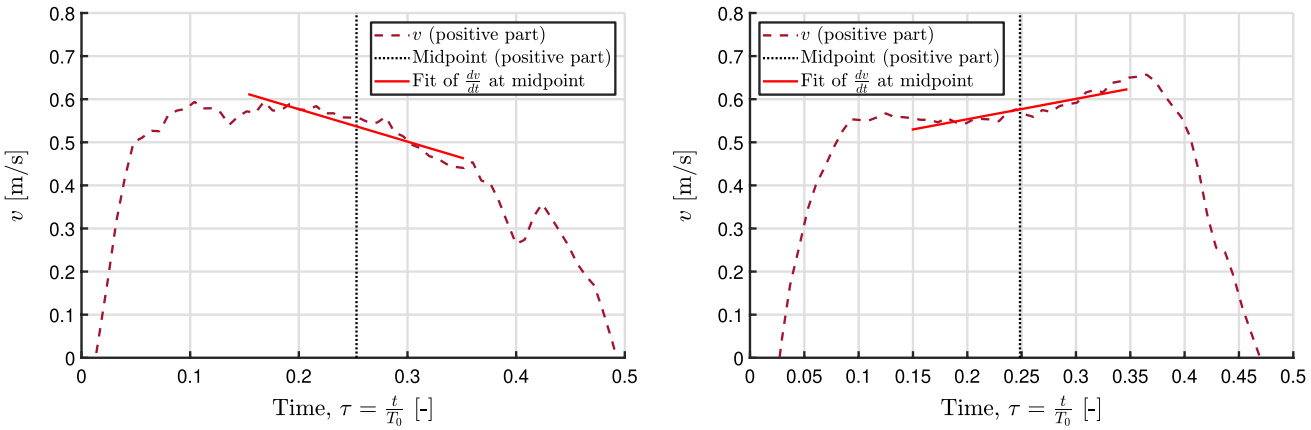

(a) $\theta_0 = 0°$ **(b)** $\theta_0 = 9.98°$

Fig. 9 Mean acceleration $\frac{\mathrm{dv}}{\mathrm{dt}}$ of the flow for the positive half of two velocity profiles from experiments with identical parameters (i.e. f, h_0, and U_∞) save for pitch amplitude. The fit used to compute the mean acceleration is shown as a solid red line. The slope of the line quantifies the relative bias of the profiles, and thereby the deviation from the ideal, symmetric case

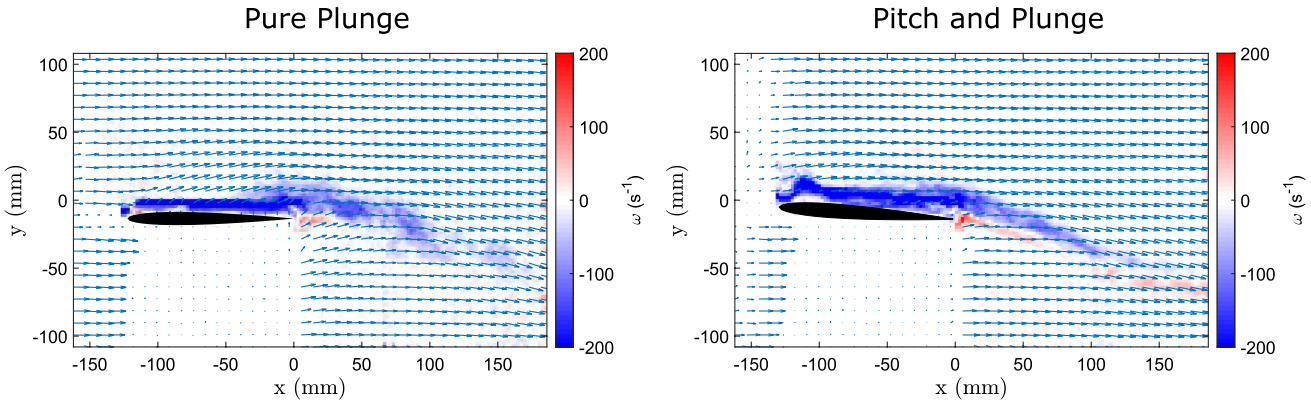

Fig. 10 Vorticity fields (taken from Round 1 of experiments) for the same cases as shown in Fig. 9, at $t/T_0 = 0.2$. Noise under the airfoil (due to the airfoil's shadow) and on the left side of the frame (due to insufficient illumination by the laser sheet) has been masked for clarity. The regularizing effect of pitch on the vorticity shed by the airfoil is evident in this comparison

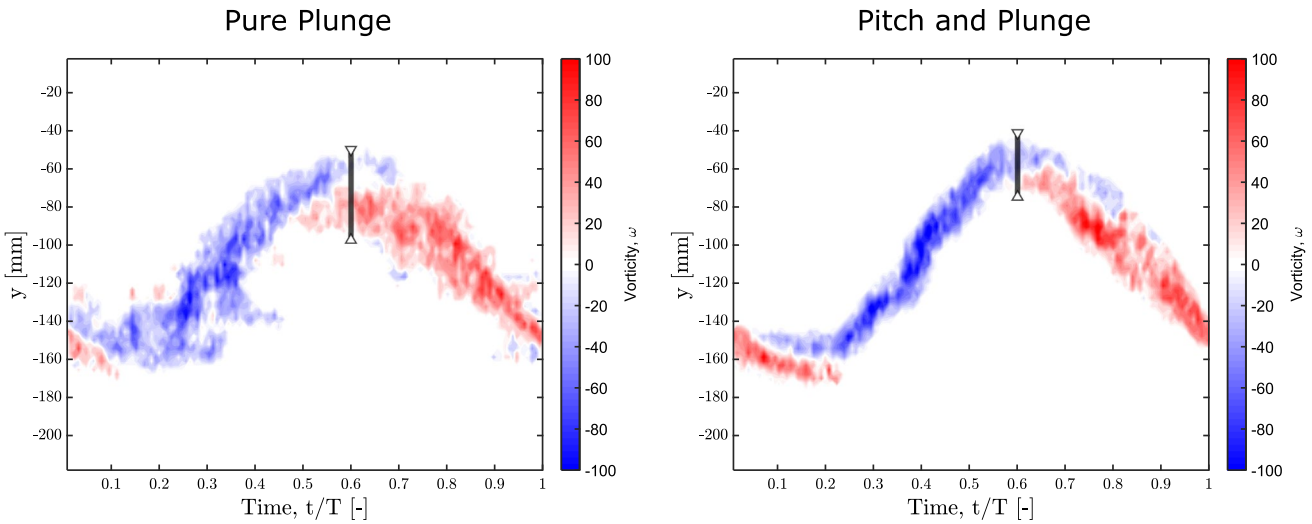

Fig. 11 Phase-averaged wake profiles at $x = 1.0c$ behind the trailing edge of the airfoil, taken from the cases shown in Fig. 10. The wake widths δ_{wake} are shown qualitatively by a gray vertical line at a single time instant in these profiles; the values of the wake width given in Fig. 12 were averaged over the entire period

into the gust profiles. Pitch created asymmetries in the opposite sense when significant leading-edge motion of the airfoil was avoided. A phase offset of 180° between pitch and plunge, so that the leading edge of the airfoil moved through a smaller amplitude than the trailing edge, combined these considerations. This was thus selected as the ideal set of kinematics for periodic-gust generation. A schematic of these kinematics is given in Fig. 8. These kinematics are identical to those identified in Sect. 2.2 by means of physical and analytical arguments.

4.2 Generation of gusts with controlled character

With the concurrence of theory and experiments in defining a set of kinematics for gust generation, it was then possible to test the specific predictions of the analytical theory in relation to the gust-generation problem. First, a series of intermediate steps in the metrics described in Sect. 3.2 are shown to demonstrate the effect of adding pitch out of phase with plunge. In Fig. 9, the positive half of the waveform for a case with $\theta_0 = 0°$ (Fig. 9a) is compared with the corresponding section for a case with $\theta_0 = 9.98°$. The addition of pitch reversed the sign of the average acceleration around the midpoint of the profile, further suggesting that, with the right pitch amplitude, the acceleration at the midpoint could be controlled to be zero—in other words, the symmetry of the gust could be controlled. For the same cases, phase-averaged vorticity fields (shown in Fig. 10) demonstrated that the structure of the wake shed off the oscillating airfoil was thinner and more organized when pitch was present. This was also reflected in the wake-width analysis, representations of which are shown in Fig. 11. These figures demonstrate the capacity of the metrics to capture physical differences in gust character within the area of interest, and also highlight the ability of phase-offset pitch to reverse some of the trends seen in the purely plunging cases.

Table 2 Kinematic parameters and corresponding optimal pitch amplitudes θ^* for the four cases shown in Figs. 12 and 13

Case	f (Hz)	h_0 (mm)	k	St	θ^*
(a)	4	20	0.603	0.032	1.91°
(b)	4	40	0.603	0.064	3.82°
(c)	4	60	0.603	0.096	5.73°
(d)	5	40	0.754	0.080	5.30°

For all cases, $U_\infty = 2.5$ m/s

Quantitative values from these two metrics were obtained for four combinations of Strouhal number and reduced frequency over a range of pitch amplitudes, in order to test the predictions of the Theodorsen theory. For a reduced frequency of $k = 0.603$, Strouhal numbers of 0.032, 0.064, and 0.096 were tested. A case with $k = 0.754$ and $St = 0.080$ was added to ensure that the theory was valid across reduced frequencies as well. These cases will be denoted as (a), (b), (c), and (d), respectively. The airfoil kinematics for these cases and corresponding optimal pitch amplitudes according to theory (θ^*) are given in Table 2.

The average wake width δ_{wake} (normalized by the thickness of the airfoil, δ_{foil}) is shown over a range of pitch amplitudes for these four cases in Fig. 12. In each case, a relative minimum in wake width was observed very close to the optimal pitch amplitude predicted by the Theodorsen

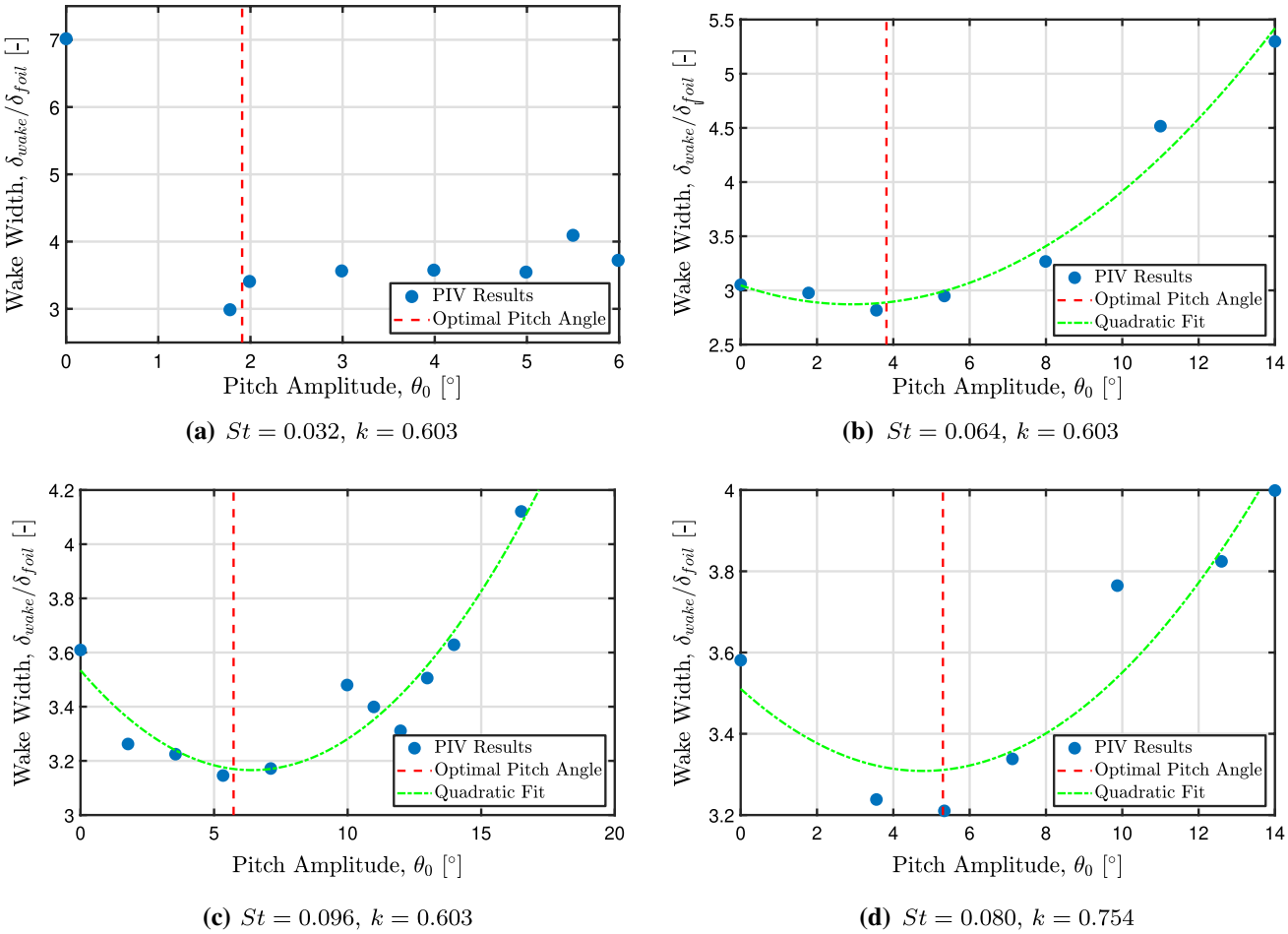

(a) $St = 0.032,\ k = 0.603$ **(b)** $St = 0.064,\ k = 0.603$

(c) $St = 0.096,\ k = 0.603$ **(d)** $St = 0.080,\ k = 0.754$

Fig. 12 Time-averaged wake width δ_{wake}, normalized by airfoil thickness δ_{foil}, of the flow at $x = 1.0c$ for four combinations of Strouhal number and reduced frequency. In each case, the airfoil is actuated in plunge with given f and h_0, and the pitch amplitude is varied. Parabolic fits are given as dashed curves to show the trends, except for case (**a**). The influence of the wake of the gust generator is minimized in all cases near the pitch amplitude θ^* prescribed by the Theodorsen theory

analysis, shown as a red vertical dashed line on each plot. The parabolic fits are only shown as guides for the eye, and are not intended to be prescriptive in any way. The effects of error in these data are more evident, stemming from the inherent noise associated with computing vorticity from velocity fields, the sensitivity of the thresholding procedure used to compute the wake width, and the fact that the field of view was so large (with respect to limits on laser power and seeding density) that achieving both sufficient illumination and sufficient resolution were difficult. Case (a), though still showing a minimum at the value of θ^* given by the Theodorsen theory, is less conclusive because of its low plunge amplitude. Inspection of the vorticity fields showed that the excursion of the airfoil, and thus the extent of the gust, was only marginally larger than the wake of the airfoil in the stationary case. As the flow in this regime was dominated by Kelvin–Helmholtz vortices from the surface of the airfoil rather than the unsteadiness of the airfoil, differences in the gust character were, therefore, much harder to measure. In spite of the influence of noise, every case investigated demonstrated general agreement with the Theodorsen theory in terms of a reduced influence of the airfoil in the downstream wake.

Measurements of the metric for gust symmetry similarly validated the predictions of the analytical theory. Figure 13 shows the mean acceleration data for each of the four cases over a range of pitch amplitudes. The prediction of the Theodorsen theory, again shown as a red vertical dashed line on each plot, coincided very well with the point where the trend of the data crossed the $\frac{\mathrm{d}v}{\mathrm{d}t}$ axis in each case, in spite of minor scatter in the data due to experimental error stemming from the limits of the apparatus and the sensitivity of the mean-acceleration metric. These results demonstrated that the gusts produced according to the Theodorsen theory were more symmetric than those produced at other pitch amplitudes.

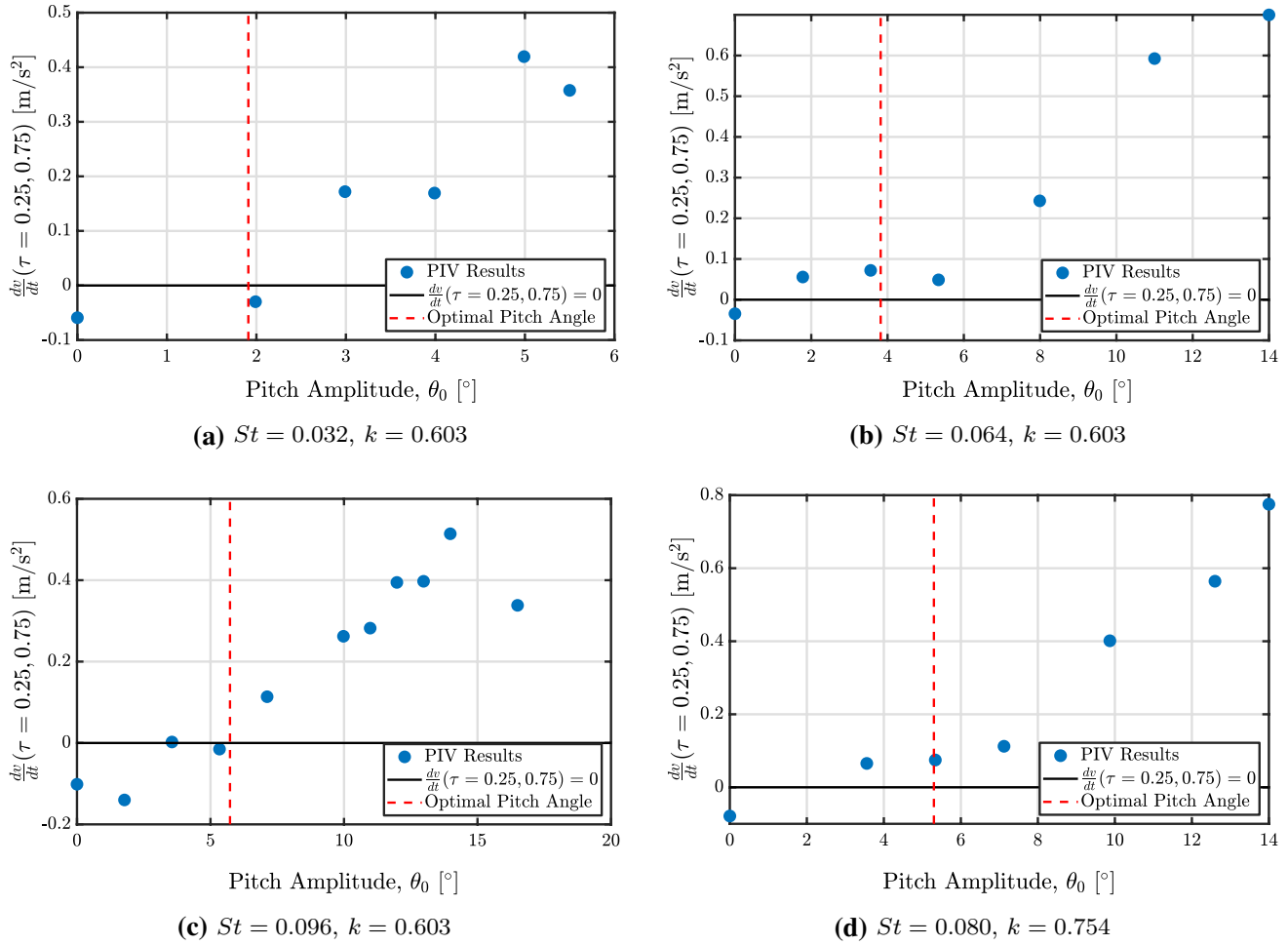

(a) $St = 0.032,\ k = 0.603$ **(b)** $St = 0.064,\ k = 0.603$

(c) $St = 0.096,\ k = 0.603$ **(d)** $St = 0.080,\ k = 0.754$

Fig. 13 Mean acceleration $\frac{\mathrm{dv}}{\mathrm{dt}}$ of the flow at $\frac{t}{T_0} = 0.25$ and $\frac{t}{T_0} = 0.75$ for four combinations of Strouhal number and reduced frequency. In each case, the airfoil is actuated in plunge with given f and h_0, and the pitch amplitude is varied. As shown by the intersection of the data trends with $\frac{\mathrm{dv}}{\mathrm{dt}} = 0$ at the red vertical dashed lines (denoting θ^*), the theory satisfactorily predicts the generation of optimally symmetric gust profiles

Table 3 Kinematic parameters and corresponding optimal pitch amplitudes θ^* for the baseline cases shown in Fig. 14a (variation in *St*) and b (variation in *k*)

Var.	f (Hz)	h_0 (mm)	k	St	θ^*	θ_0 (exp.)
St	4	20	0.603	0.032	1.91°	1.99°
St	4	30	0.603	0.048	2.86°	2.67°
St	4	40	0.603	0.064	3.82°	3.56°
St	4	50	0.603	0.080	4.77°	4.45°
St	4	60	0.603	0.096	5.73°	5.34°
St	4	70	0.603	0.112	6.68°	6.23°
k	2	100	0.302	0.080	2.84°	2.67°
k	3	66.7	0.452	0.080	3.96°	3.56°
k	4	50	0.603	0.080	4.77°	4.45°
k	5	40	0.754	0.080	5.30°	5.34°
k	6	33.3	0.905	0.080	5.59°	5.34°

The actual pitch amplitudes used in the experiments are given under θ_0 (exp.)

Finally, to more clearly demonstrate the effectiveness of the Theodorsen theory for gust generation, a range of Strouhal numbers and reduced frequencies were tested with the addition of pitch according to the theory. The values of these optimal pitch amplitudes are given in Table 3. These results could then be compared directly with the baseline

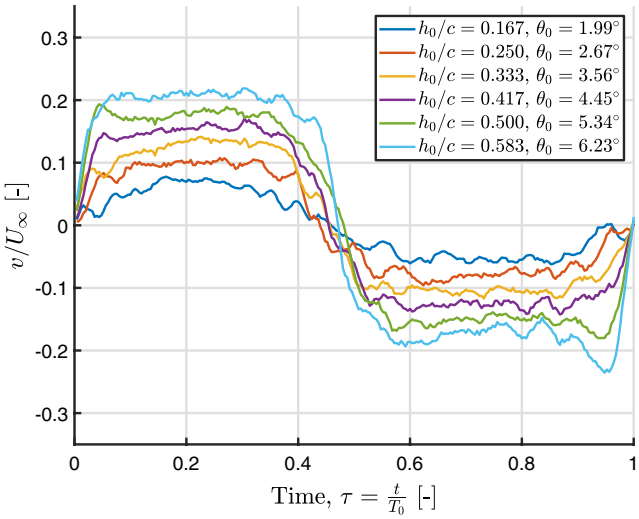

(a) $0.032 \leq St \leq 0.112$ and $k = 0.603$

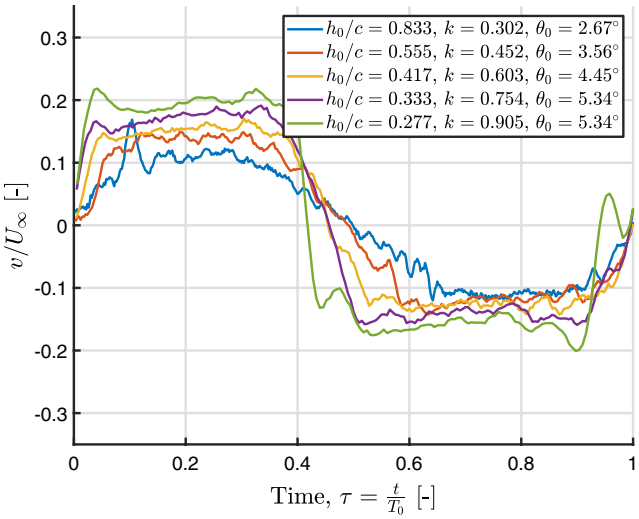

(b) $0.302 \leq k \leq 0.905$ and $St = 0.080$

Fig. 14 Profiles of v behind a pitching and plunging airfoil for a range of **a** Strouhal numbers and **b** reduced frequencies. Despite the actual pitch amplitudes being slightly lower than those prescribed by the theory (by no more than 0.45°), these curves still compare favorably in terms of symmetry and smoothness to those in Fig. 5

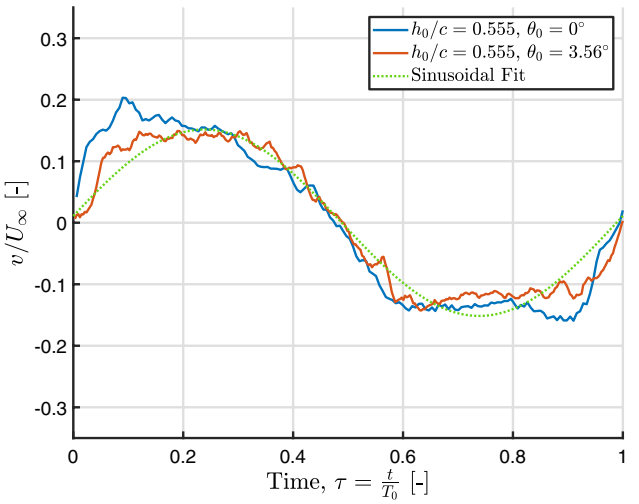

(a) Comparison case 1: $St = 0.080$ and $k = 0.452$

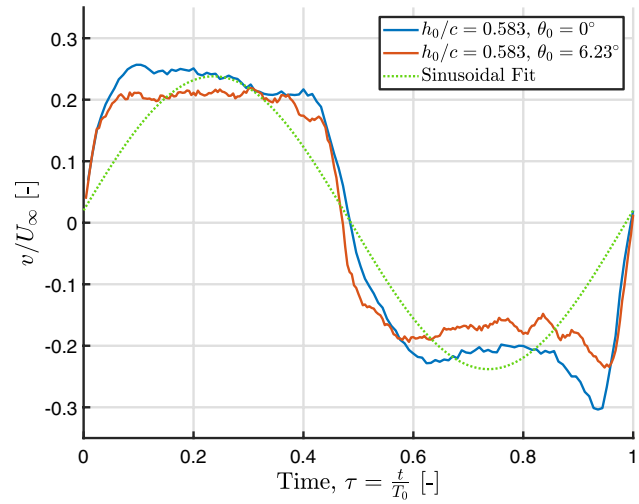

(b) Comparison case 2: $St = 0.112$ and $k = 0.603$

Fig. 15 Two comparisons of gusts generated by a plunging airfoil with and without pitching kinematics according to the Theodorsen theory. **a** shows a moderate-amplitude gust, while **b** shows the highest-amplitude gust examined in this study. A sinusoidal fit of the case with pitch is shown as a dashed line in both figures. In both cases, the addition of pitch yields curves that are more symmetric about their peaks, thus more closely representing the ideal sinusoidal gust profile. Deviations in the negative halves of the gust profiles are due to aerodynamic interference from the airfoil's actuators

cases shown in Fig. 5. Due to the process of selecting test cases for the experiments, the pitch amplitudes tested in the experiments were not precisely equivalent to those supplied by the theory, differing at most by 0.45° (less than 7% of the optimal pitch amplitude). These differences, recorded in Table 3, were not large enough to significantly affect the experimental results. The optimized gust profiles—shown in Fig. 14—showed significant improvement in control over the waveform shape, in comparison to the baseline cases. The leftward shift of the maxima visible in Fig. 5a for the cases of pure plunge was essentially removed for all cases in Fig. 14a. At higher reduced frequencies, shown in Fig. 14b, a slight rightward bias became evident, likely an effect of an earlier roll-up of shear-driven instabilities due to the more

dramatic motions of the airfoil, which are not taken into account by the theoretical predictions. These limiting effects will be discussed further in Sect. 4.3. Overall, the addition of pitch according to theory regularized the vertical-velocity profiles over a range of Strouhal numbers and reduced frequencies, making the resultant gusts more uniform in shape and less affected by the wake of the airfoil generating the gust.

4.3 Evaluation and discussion

To highlight the differences between the baseline cases and the final gust-generation cases, two direct comparisons are shown in Fig. 15, in addition to fits of sine waveforms to the gust-generation cases. These comparisons highlight the influence of pitch in making the gust profiles more symmetric about their peaks. In these cases as well, the presence of pitch seemed to reduce the influence of velocity spikes in the profiles, which are likely artifacts of vortex shedding from the airfoil. This aligns with the wake mitigation shown previously in Fig. 12. For moderate combinations of St and k, such as that shown in Fig. 15a, the gust profiles were very close to sinusoidal. Most notably, the regularizing effect of pitch according to the prescriptions of theory, in terms of gust symmetry and smoothness, was still significant for the highest-amplitude gusts produced in this study (shown in Fig. 15b).

Thus, the gust-generation protocol presented in this work was able to produce high-amplitude gusts without losing control over the character of their waveforms. The generated gusts were also significantly higher in amplitude (up to 13.8°) and reduced frequency (up to $k = 0.905$) than those produced by generators with the same number of actuators (e.g. Lancelot et al. 2015; Wood et al. 2017), as well as more complex systems with multiple vanes (e.g. Saddington et al. 2015; Wei et al. 2019). A more detailed comparison of the performance of the gust generator with those found in the literature is presented in Table 4. This gust-generation scheme is thus well-suited for experiments involving highly dynamic inflow conditions. Since the derivation for θ^* showed that the optimal pitch amplitude was not a function of Reynolds number, it is also expected that the gust generator will perform well across a wide range of Reynolds

Table 4 Comparison of the reduced-frequency ranges and maximum gust-angle amplitudes ($\hat{\alpha}_G$) of several gust-generation mechanisms in the literature with the one presented in the present study

Gust-generation study	k range	Max $\hat{\alpha}_G$
Hakkinen and Richardson (1957)	0.1–0.2	0.3°
Bennett and Gilman (1966)	0.08–0.34	1.4°
Jancauskas and Melbourne (1980)	0.08–2.5	11°
Saddington et al. (2015)	0.02–0.1	12°
Lancelot et al. (2015)	0.04–0.19	7°
Wood et al. (2017)	0.12–1.2	7°
Wei et al. (2019)	0.09–0.42	12°
Present study	0.30–0.90	13.8°

Here, k is defined by the length of the gust generator in each study, and not a downstream test profile

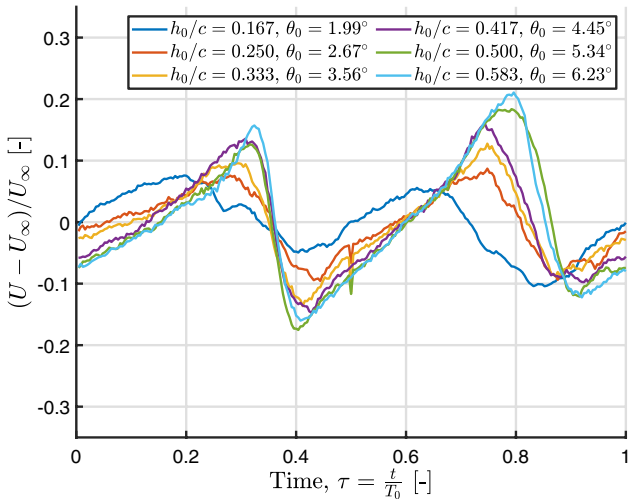

(a) Fluctuations in the streamwise velocity u, for the cases from Fig. 14a

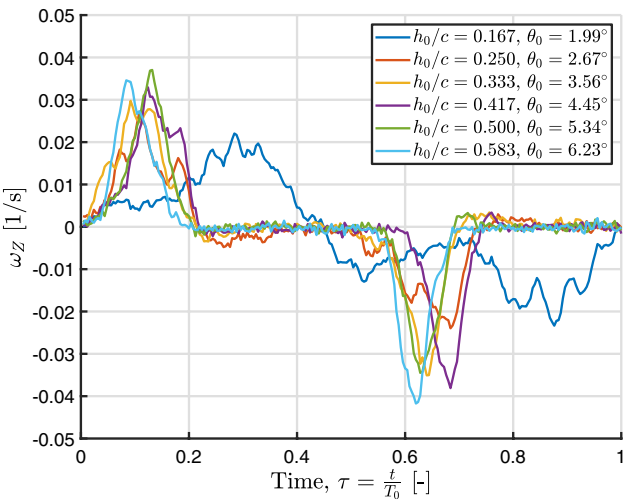

(b) Profiles of the z-vorticity ω_z, for the cases from Fig.14a

Fig. 16 Phase-averaged profiles of **a** fluctuations in u and **b** spanwise vorticity ω_z for the cases shown in Fig. 14a. The fluctuations in u remain small compared to U_∞. For all cases except the smallest plunge amplitude, the influence of vorticity is limited to brief periods where the wake of the gust generator passes through the region of interest

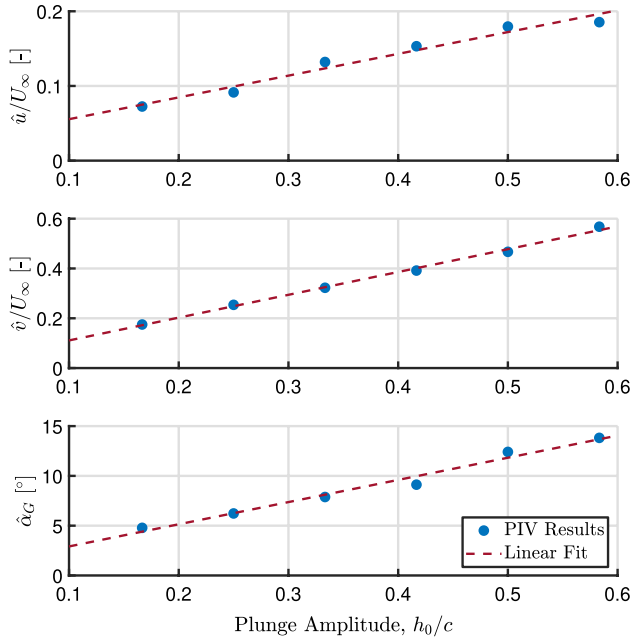

Fig. 17 Amplitudes of the fluctuations in u, v, and α_G from the cases presented in Fig. 14a, which all increase linearly with h_0. These linear trends are expected from the behavior of the idealized gust generator outlined in Sect. 2.2, and imply that the apparatus operated sufficiently close to the ideal gust-generation scenario

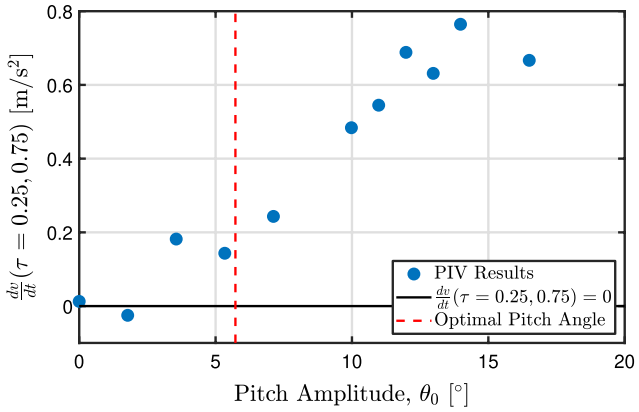

Fig. 18 Mean acceleration $\frac{dv}{dt}$ of the flow at $\frac{t}{T_0} = 0.25$ and $\frac{t}{T_0} = 0.75$ for $St = 0.096$ and $k = 0.603$ (from Fig. 13c), measured at $x = 1.5c$ downstream of the airfoil's trailing edge. The data are uniformly shifted up by approximately 0.1 m/s^2, compared to the measurements at $x = 1.0c$

numbers, especially since high Reynolds numbers generally imply significantly lower values of k and St.

To complete the characterization of the gust-generation apparatus, it is instructive to examine briefly the effects of the gust generator on the streamwise-velocity and vorticity fluctuations in the region of interest. The streamwise-velocity profiles and vorticity profiles corresponding to the cases shown in Fig. 14a are presented in Fig. 16a, b, respectively. The streamwise velocity fluctuations also increased linearly in amplitude ($\hat{u}$) with the plunge amplitude h_0, as shown in Fig. 17. In each case, the amplitude of these fluctuations was about one third of the amplitude of the vertical velocity fluctuations ($\hat{v}$). This was expected from the operating principle of the gust generator, which ideally would redirect the incoming flow in a sinusoidal fashion with minimal disturbance of the flow properties themselves. This kind of flow redirection necessitates fluctuations of $\hat{u}$ that scale with $\hat{v}$ and the gust-angle amplitude $\hat{\alpha}_G$, a relationship that is captured well in the experimental data presented in Fig. 17. These data implied that the gust generator was able to produce disturbances in a similar fashion to the ideal gust generator outlined in Sect. 2.2. Overall, the fluctuations in u comprised only a small fraction of the free-stream velocity, and thus did not significantly influence the character of the angle-of-attack variations, which were dominated by v.

The vorticity profiles shown in Fig. 16b were also well-conditioned for the gust-generation problem. In all cases except that involving the lowest tested plunge amplitude ($h_0/c = 0.167$), the vorticity remained zero for most of the period. This meant that the influence of the wake of the gust generator was minimized not only in its spatial extent, as shown previously in Fig. 12, but also in its temporal significance. At the lowest plunge amplitude, the motion of the airfoil was not large enough for the airfoil's wake to clear the region of interest at any time, since h_0/c in this case was around twice δ_{foil}/c, and thus the Kelvin-Helmholtz instabilities shed by the airfoil always passed through the ROI. These observations validate the argument made previously, based on the work of Hufstedler and McKeon (2019), that employing plunge kinematics can mitigate the influence of the wake of the airfoil on the gusts it produces. The complete removal of the influence of the airfoil's wake is impossible for airfoils of finite thickness, but these results demonstrate that it is possible to limit these effects to short intervals within the gust period.

Until now, all analyses have been carried out at a point one chord length behind the gust-generating airfoil. To project how the gust properties would change further downstream, the point furthest downstream from the airfoil in the measurement domain (at $x = 1.5c$ behind the trailing edge) was considered. Admittedly, this was not much farther downstream than the original test case, but restrictions on optical access for the laser sheet in the wind tunnel prohibited the acquisition of PIV measurements at larger downstream distances. For the sake of brevity, only the case of $St = 0.096$ and $k = 0.603$ from Fig. 13c is presented here. The corresponding data generated from the $x = 1.5c$ location for the mean accelerations are shown in Fig. 18. These data retain their shape but are shifted up in value by approximately 0.1 m/s^2 compared to the corresponding data from

$x = 1.0c$. This would suggest that the value of θ_0 needed to produce symmetric gusts at this downstream location would need to be slightly lower than that predicted by theory. Other than this slight asymmetry, the gust profiles measured at this location do not appear any less smooth or less regular than their upstream counterparts. The reason for this small deviation from the predictions of the theory most likely lies in the influence of viscous effects in the wake. The Theodorsen theory only accounts for the wake circulation of the airfoil, and is not concerned with the properties of the global flow field further downstream of the airfoil. It is thus not surprising that instabilities, such as shear-layer roll-up due to velocity gradients in the gust, would lead to more complex dynamics as the flow develops further downstream. These roll-up effects were observed in smoke-wire visualizations, but could not be quantified using PIV because of the aforementioned limitations of the experimental setup. This "drift" of the gust profiles toward asymmetry with increased downstream distance from the gust generator would require additional analytical and experimental work to quantify and correct against. With regard to the present study, however, it is sufficient to note that this deviation was relatively small and does not affect the smoothness or controllability of the gust profiles. Furthermore, the viscous dynamics responsible for these effects will be attenuated in influence at higher Reynolds numbers. Therefore, the deviation from the predictions of the theory, while interesting from a fluid-mechanics standpoint, should not greatly affect the efficacy of the gust-generation scheme presented here.

5 Conclusions

In this work, considerations have been outlined for the generation of gusts with carefully controlled character using a single airfoil actuated in plunge and pitch. The Theodorsen theory for unsteady aerodynamics was used to predict the pitch amplitude necessary to produce smooth, symmetric gusts at a given Strouhal number and reduced frequency. The validity of the theory was supported both by physical arguments and by experimental investigations. The quantitative predictions given by the theory were then confirmed in experiments that measured the symmetry of the vertical-velocity profiles produced in the wake of the airfoil, and the extent of the wake of the airfoil itself within the gust region. The gust signals produced were reasonably smooth, and reached significantly higher amplitudes and reduced frequencies than those attained by other gust-generation methods. For low to moderate Strouhal numbers and reduced frequencies, the gusts produced were very close to sinusoidal; the gusts remained smooth and symmetric even at the highest values of St and k examined in this work. In addition to the vertical-velocity fluctuations, the effects of the gust generator on the streamwise velocity and spanwise vorticity were also quantified, and the evolution of the gust profiles at measurement locations further downstream from the airfoil was evaluated. The results of this work suggest that the physics of the gust-generation problem do not require high degrees of mechanical complexity to solve, but rather can be manipulated as needed with just a single airfoil and potential flow theory.

Additional steps could be taken to improve the quality of the gust flows produced in the wake of the airfoil. Employing airfoil actuators that do not protrude into the center of the test section would greatly regularize the quality of the gust in the negative portion of the profile. A thinner airfoil, built from a less flexible material, would produce an even thinner wake, and could also be actuated more reliably over a wider range of kinematics. Measurement of the forces and moments on the airfoil would also be of interest, to see more quantitatively how unsteady loads may be reduced by these kinds of kinematics. Force measurements would also allow the effect of pitch phase, which was not thoroughly explored in this work, to be more rigorously determined. Specifically, changing the pitch phase using non-sinusoidal actuation waveforms (or, perhaps more easily, with independent pitch and plunge actuators) would allow the true minimum for the pitching moment ($\hat{M}^*_\theta = 0$) to be realized and validated. Lastly, tests at higher Reynolds numbers would allow the gust generator to be used in larger-scale experiments.

These findings have significant implications not only for the generation of well-defined gusts in aerodynamics experiments, but also for the aerodynamic behavior of tandem-wing configurations, for example in dragonfly wings, or on a larger scale, within flocks of birds or schools of fish. The control of wake structures purely by kinematics could also apply to gust-load alleviation in rotorcraft and biologically inspired unmanned aerial vehicles (UAVs). It is important to note, however, that the trends shown in this study will break down at higher Strouhal numbers and reduced frequencies, where dynamic effects become unavoidable. Nevertheless, a foray into this sector of the parameter space would allow the results of this work to be generalized to a much wider range of applications in aerodynamics, flow control, biological propulsion, and other related fields.

Acknowledgements The authors wish to acknowledge financial support of this study by the Sino-German Center and the Deutsche Forschungsgemeinschaft through the Project TR 194/55-1: "Flow Control for Unsteady Aerodynamics of Pitching/Plunging Airfoils". In addition, author Nathaniel Wei was supported by the German-American Fulbright Commission with a Grant in the Student Category during his stay at the TU Darmstadt. The authors would also like to extend their appreciation to the workshop staff for their assistance and professional support in the preparation of the wind tunnel and test airfoil for these experiments, and to Stefan Trieß, who characterized and optimized the linear actuators.

References

Anderson JM, Streitlien K, Barrett DS, Triantafyllou MS (1998) Oscillating foils of high propulsive efficiency. J Fluid Mech 360:41–72

Atassi HM (1984) The Sears problem for a lifting airfoil revisited—new results. J Fluid Mech 141:109–122. https://doi.org/10.1017/S0022112084000768

Bennett RM, Gilman J (1966) A wind-tunnel technique for measuring frequency-response functions for gust load analyses. J Aircr 3(6):535–540. https://doi.org/10.2514/3.43773

Brion V, Lepage A, Amosse Y, Soulevant D, Senecat P, Abart JC, Paillart P (2015) Generation of vertical gusts in a transonic wind tunnel. Exp Fluids 56(7):145. https://doi.org/10.1007/s00348-015-2016-5

Carr LW (1988) Progress in analysis and prediction of dynamic stall. J Aircr 25(1):6–17. https://doi.org/10.2514/3.45534

Cekli HE, van de Water W (2010) Tailoring turbulence with an active grid. Exp Fluids 49(2):409–416. https://doi.org/10.1007/s00348-009-0812-5

Cordes U, Kampers G, Meißner T, Tropea C, Peinke J, Hölling M (2017) Note on the limitations of the Theodorsen and Sears functions. JFluid Mech. https://doi.org/10.1017/jfm.2016.780

Efron B (1979) Bootstrap methods: another look at the Jackknife. Ann Stat 7(1):1–26. https://doi.org/10.1214/aos/1176344552

Ekaterinaris JA, Platzer MF (1998) Computational prediction of airfoil dynamic stall. Prog Aerosp Sci 33(11):759–846. https://doi.org/10.1016/S0376-0421(97)00012-2

Gharali K, Johnson DA (2013) Dynamic stall simulation of a pitching airfoil under unsteady freestream velocity. J Fluids Struct 42:228–244. https://doi.org/10.1016/j.jfluidstructs.2013.05.005

Goldstein ME, Atassi H (1976) A complete second-order theory for the unsteady flow about an airfoil due to a periodic gust. J Fluid Mech 74(4):741–765. https://doi.org/10.1017/S0022112076002036

Griffin KP, Wei NJ, Bodenschatz E, Bewley GP (2019) Control of long-range correlations in turbulence. Exp Fluids 60(4):55. https://doi.org/10.1007/s00348-019-2698-1

Hakkinen RJ, Richardson AS (1957) Theoretical and experimental investigation of random gust loads. Part I: aerodynamic transfer function of a simple wing configuration in incompressible flow. NACA Tech. Rep. 3878

Ham ND, Bauer PH, Lawrence TL (1974) Wind tunnel generation of sinusoidal lateral and longitudinal gusts by circulation of twin parallel airfoils. Tech. Rep. NASA CR 137547

Hufstedler EAL, McKeon BJ (2019) Vortical gusts: experimental generation and interaction with wing. AIAA J 57(3):921–931. https://doi.org/10.2514/1.J056914

Jancauskas ED, Melbourne WH (1980) The measurement of aerodynamic admittance using discrete frequency gust generation. In: Proceedings of the 7th Australasian hydraulics and fluid mechanics conference, Brisbane, Australia

Jancauskas ED, Melbourne WH (1986) The aerodynamic admittance of two-dimensional rectangular section cylinders in smooth flow. J Wind Eng Ind Aerodyn 23:395–408. https://doi.org/10.1016/0167-6105(86)90057-7

Klein S, Hoppmann D, Scholz P, Radespiel R (2014) High-lift airfoil interacting with a vortical disturbance: wind-tunnel measurements. AIAA J 53(6):1681–1692. https://doi.org/10.2514/1.J053441

Klein S, Scholz P, Radespiel R (2017) A two-element high-lift airfoil in disturbed flow conditions. CEAS Aeronaut J 8(1):79–91. https://doi.org/10.1007/s13272-016-0221-4

Knebel P, Kittel A, Peinke J (2011) Atmospheric wind field conditions generated by active grids. Exp Fluids 51(2):471–481. https://doi.org/10.1007/s00348-011-1056-8

Lancelot PMGJ, Sodja J, Werter NPM, De Breuker R (2015) Design and testing of a low subsonic wind tunnel gust generator. Proceedings of the 16th international forum on aeroelasticity and structural dynamics, IFASD 2015, St Petersburg (Russia), 28 June-2 July, 2015; Authors version

Larose GL (1999) Experimental determination of the aerodynamic admittance of a bridge deck segment. J Fluids Struct 13(7):1029–1040. https://doi.org/10.1006/jfls.1999.0244

Lysak PD, Capone DE, Jonson ML (2016) Measurement of the unsteady lift of thick airfoils in incompressible turbulent flow. J Fluids Struct 66:315–330. https://doi.org/10.1016/j.jfluidstructs.2016.07.018

Makita H (1991) Realization of a large-scale turbulence field in a small wind tunnel. Fluid Dyn Res 8(1–4):53. https://doi.org/10.1016/0169-5983(91)90030-M

McGowan GZ, Granlund K, Ol MV, Gopalarathnam A, Edwards JR (2011) Investigations of lift-based pitch-plunge equivalence for airfoils at low Reynolds numbers. AIAA J 49(7):1511–1524. https://doi.org/10.2514/1.J050924

Prangemeier T, Rival D, Tropea C (2010) The manipulation of trailing-edge vortices for an airfoil in plunging motion. J Fluids Struct 26(2):193–204. https://doi.org/10.1016/j.jfluidstructs.2009.10.003

Raffel M, Willert CE, Wereley S, Kompenhans J (2007) Particle image velocimetry: a practical guide, 2nd edn. Springer, Berlin

Rival D, Prangemeier T, Tropea C (2009) The influence of airfoil kinematics on the formation of leading-edge vortices in bio-inspired flight. Exp Fluids 46(5):823–833. https://doi.org/10.1007/s00348-008-0586-1

Rival D, Schönweitz D, Tropea C (2011) Vortex interaction of tandem pitching and plunging plates: a two-dimensional model of hovering dragonfly-like flight. Bioinspir Biomim 6(1):016008. https://doi.org/10.1088/1748-3182/6/1/016008

Saddington A, Finnis M, Knowles K (2015) The characterisation of a gust generator for aerodynamic testing. Proc Inst Mech Eng Part G J Aerosp Eng 229(7):1214–1225. https://doi.org/10.1177/0954410014548237

Sears WR (1941) Some aspects of non-stationary airfoil theory and its practical application. J Aeronaut Sci 8(3):104–108. https://doi.org/10.2514/8.10655

Tang DM, Cizmas PGA, Dowell EH (1996) Experiments and analysis for a gust generator in a wind tunnel. J Aircr 33(1):139–148. https://doi.org/10.2514/3.46914

Theodorsen T (1934) General theory of aerodynamic instability and the mechanism of flutter. Technical Report 496, National Advisory Committee for Aeronautics

Tropea C, Yarin A, Foss JF (eds) (2007) Springer handbook of experimental fluid mechanics. Springer, Berlin

Visbal MR (2011) Numerical investigation of deep dynamic stall of a plunging airfoil. AIAA J 49(10):2152–2170. https://doi.org/10.2514/1.J050892

Wei NJ, Kissing J, Wester TTB, Wegt S, Schiffmann K, Jakirlic S, Hölling M, Peinke J, Tropea C (2019) Insights into the periodic gust response of airfoils. J Fluid Mech 876:237–263. https://doi.org/10.1017/jfm.2019.537

Widmann A, Tropea C (2015) Parameters influencing vortex growth and detachment on unsteady aerodynamic profiles. J Fluid Mech 773:432–459. https://doi.org/10.1017/jfm.2015.259

Wood KT, Cheung RC, Richardson TS, Cooper JE, Darbyshire O, Warsop C (2017) A new gust generator for a low speed wind tunnel: design and commissioning. In: 55th AIAA Aerospace Sciences Meeting, AIAA SciTech Forum, American Institute of Aeronautics and Astronautics. https://doi.org/10.2514/6.2017-0502

Affiliations

Nathaniel J. Wei[1,2] · Johannes Kissing[1] · Cameron Tropea[1]

[1] Institute for Fluid Mechanics and Aerodynamics, Technische Universität Darmstadt, Alarich-Weiss-Strasse 10, 64287 Darmstadt, Germany

[2] Department of Mechanical Engineering, Stanford University, Stanford, CA 94305, USA